Author Contributions:

Conceptualization: S. A. Drake, C. K. Thomas
Data curation: C. K. Thomas
Formal analysis: S. A. Drake
Funding acquisition: C. K. Thomas
Investigation: S. A. Drake, C. K. Thomas
Methodology: S. A. Drake, C. K. Thomas
Project Administration: C. K. Thomas
Resources: S. A. Drake
Software: S. A. Drake
Validation: S. A. Drake

Increasing Daytime Stability Enhances Downslope Moisture Transport in the Subcanopy of an Even-Aged Conifer Forest in Western Oregon, USA

S. A. Drake[1,2] , D. E. Rupp[2,3], C. K. Thomas[2,4] , H. J. Oldroyd[5] , M. Schulze[6] , and J. A. Jones[2]

[1]Department of Physics, University of Nevada, Reno, NV, USA, [2]College of Earth, Ocean, and Atmospheric Sciences, Oregon State University, Corvallis, OR, USA, [3]Oregon Climate Change Research Institute, College of Earth, Ocean, and Atmospheric Sciences, Oregon State University, Corvallis, OR, USA, [4]Micrometeorology, University of Bayreuth, Bayreuth, Germany, [5]Department of Civil and Environmental Engineering, University of California, Davis, CA, USA, [6]College of Forestry, Oregon State University, Corvallis, OR, USA

Abstract Mountain breezes, including katabatic and anabatic flows, and temperature inversions are common features of forested mountain landscapes. However, the effects of mountain breezes on moisture transport in forests and implications for regional climate change are not well understood. A detailed, instrumented study was conducted from July to September 2012 in an even-aged conifer forest in the Oregon Cascade Range to investigate how temperature profiles within the forest canopy influenced atmospheric surface layer processes that ventilate the forest. Subcanopy inversion strength has a bimodal relationship to subcanopy wind speed and moisture flux from the forest. On days with relatively modest heating of the top of the canopy and weak subcanopy inversions, above canopy winds more efficiently mix subcanopy air, leading to greater than average vertical moisture flux and weaker than average along-slope, subcanopy water vapor advection. On days with strong heating of the top of the canopy and a strong subcanopy inversion, vertical moisture flux is suppressed, and daytime downslope winds are stronger than average under the canopy. Increased downslope winds lead to increased downslope transport of water vapor, carbon dioxide, and other scalars under the canopy. Increasing summer vapor pressure deficit in the Pacific Northwest will enhance both processes: vertical moisture transport by mountain breezes when subcanopy inversions are weak and downslope water vapor transport when subcanopy inversions are strong. These mountain breeze dynamics have implications for climate refugia in forested mountains, forest plantations, and other forested regions with a similar canopy structure and regional atmospheric forcings.

Plain Language Summary The summer and fall seasons in the Pacific Northwest are typically warm and dry, and solar radiation and locally generated breezes affect temperature and moisture content of air under the forest canopy. In forest plantations, which have uniform height, the sun heats the canopy and creates an inversion—an increase in temperature with height under the forest canopy. On days with strong canopy heating, this inversion limits moisture loss through the top of the canopy and enhances winds that flow downslope below the canopy, carrying moisture out of the system. On days with less canopy heating, winds mix air above and within the canopy and promote moisture loss to the air above the forest canopy. Regional models of future climate simulate declining dry-season relative humidity. Collectively, these findings indicate that future climate will enhance both vertical and downslope moisture loss during the dry season from forest plantations, which represent a large fraction of forest cover of the Pacific Northwest of the USA.

1. Introduction

An increasing fraction of global forest area consists of plantation forests (Hansen et al., 2013). Plantations typically are even-aged with a single species and simple canopy structure (Lefsky et al., 1999). Past management practices have led to millions of acres of dense, uniform stands on federal forests, and private land in the Pacific Northwest (PNW) where conifer forests are the predominant land-cover in mountainous terrain. Several recent studies have reported that even-aged conifer forests evapotranspire more water than reference, native, multistoried forests during the dry summers in the PNW and British Columbia, Canada (Gronsdahl et al., 2019; Perry & Jones, 2017; Segura et al., 2020), with potential implications for regional water supply (Jones & Hammond, 2020). Yet despite

Visualization: S. A. Drake
Writing – original draft: S. A. Drake
Writing – review & editing: S. A. Drake, D. E. Rupp, C. K. Thomas, H. J. Oldroyd, M. Schulze, J. A. Jones

the important role of forest plantations in mediating land cover responses to climate change, the effects of forest plantation canopy structure on atmospheric flows of heat and moisture are not well understood.

Forest canopy structure affects through-canopy mixing and therefore sensible heat and moisture fluxes (Freundorfer et al., 2019; Thomas et al., 2013). Studies have shown that maximum air temperature and vapor pressure deficit are lower under forest canopies than nearby unforested areas (Ferrez et al., 2011; Karlsson, 2000). The forest water balance plays a key role in buffering forest response to warming and increased vapor pressure deficit (Davis et al., 2019). Regional climate processes and local terrain produce areas of relatively cool temperature in forested mountains, which have been described as "microrefugia" (Dobrowski, 2011; Lenoir et al., 2017). Many recent studies have attempted to model subcanopy temperature (e.g., Holden et al., 2016; Lembrechts & Lenoir, 2020). Yet observational studies of heat and moisture transfer in forest canopies are lacking (de Frenne et al., 2021; Thomas, 2011). A better understanding of subcanopy heat and moisture transport is relevant to topics as diverse as cold air pooling, moisture transport and losses, and wildfires (Daly et al., 2010; Davis et al., 2017; Frey et al., 2016; Richie et al., 2007).

Temperature inversions are frequent in forested mountains, even during daytime in summer (Daly et al., 2010; Minder et al., 2010; Rupp et al., 2020). Landscape-scale inversions and cold air pooling result from differential landscape heating (e.g., Lundquist et al., 2008). In addition, heating of the forest canopy influences temperature gradients and moisture exchange (Brutsaert & Parlange, 1992; Leuzinger & Körner, 2007) and contributes to the formation of an inversion within the canopy, especially under the uniform canopy structure of a plantation forest (Hosker et al., 1974). Subcanopy inversions modulate the influence of above-canopy winds on the subcanopy by limiting vertical mixing into the subcanopy (Launiainen et al., 2007; Thomas & Foken, 2007). Subcanopy inversions tend to weaken during the night (Juang et al., 2006; Whiteman, 1982) and reestablish and strengthen during the day (Froelich & Schmid, 2006; Raynor, 1971; Staebler & Fitzjarrald, 2005; Tóta et al., 2012). Although models have explored how forest canopy structure influences air flows in mountain valleys (Kiefer & Zhong, 2013, 2015), few studies have examined the interaction between subcanopy temperature inversions and airflow within forest canopies in mountain landscapes.

The objective of this study is to determine how summertime heating of the canopy of a dense plantation forest influences transport of heat and moisture into, out of, and within the forest canopy in a steep mountain watershed, which is typical of much of the PNW of the USA. The study quantified subcanopy atmospheric processes in a 45-year-old plantation forest characterized by a uniform single-layer canopy during the summer dry season when plants are drought stressed and therefore more sensitive to subtle environmental changes (Hughes, 2000). Subcanopy flow regimes are then examined in the context of regional climate change predictions over PNW forests to investigate the feedback between canopy heating and subcanopy moisture transport.

2. Materials and Methods

2.1. Study Site

The study was conducted from July to September of 2012 in a subbasin of Lookout Creek (64 km²), in the HJ Andrews Experimental Forest (HJ Andrews), and Long-Term Ecological Research (LTER) site in the central western Cascades of Oregon, USA (122.25°W, 44.21°N). Slope gradients range from 30% to more than 60% in the HJ Andrews, and steep tributary valleys, such as the study site, drain to a central valley. Mean annual temperature in the HJ Andrews is 9.7°C and mean annual precipitation is 2350 mm. Less than 5% of precipitation occurs during the dry season (July 1 to September 30) (Harr, 1983). The study site was Watershed 1 (WS1, Figure 1), a relatively small (96 ha), steep (average slope ~60%) northwest facing valley near the outlet of Lookout Creek Basin. WS1 is an example of forest plantations that were established after clear-cutting of old-growth forest on federal forest land, mostly between 1945 and 1990. Old-growth logging on federal forest land largely ceased in the PNW after 1990, and logging on federal forest land since 1990 in the PNW has been largely restricted to thinning of these forest plantations (Spies et al., 2019). WS1 was chosen as the study site because it is a 45-year-old conifer plantation characterized by a uniform single-layer canopy in a steep mountain watershed, and it is typical of managed forests that occupy the majority of forest lands in the PNW of the USA.

Elevation ranges from 460 to 990 m in WS1 and from 430 to >1600 m in Lookout Creek. The original vegetation of WS1, old growth Douglas-fir (Pseudotsuga menziesii) (150–500 years), was clear-cut and cable yarded between 1962 and 1966, and the remaining slash was subsequently broadcast burned in 1966 (Fredricksen, 1970;
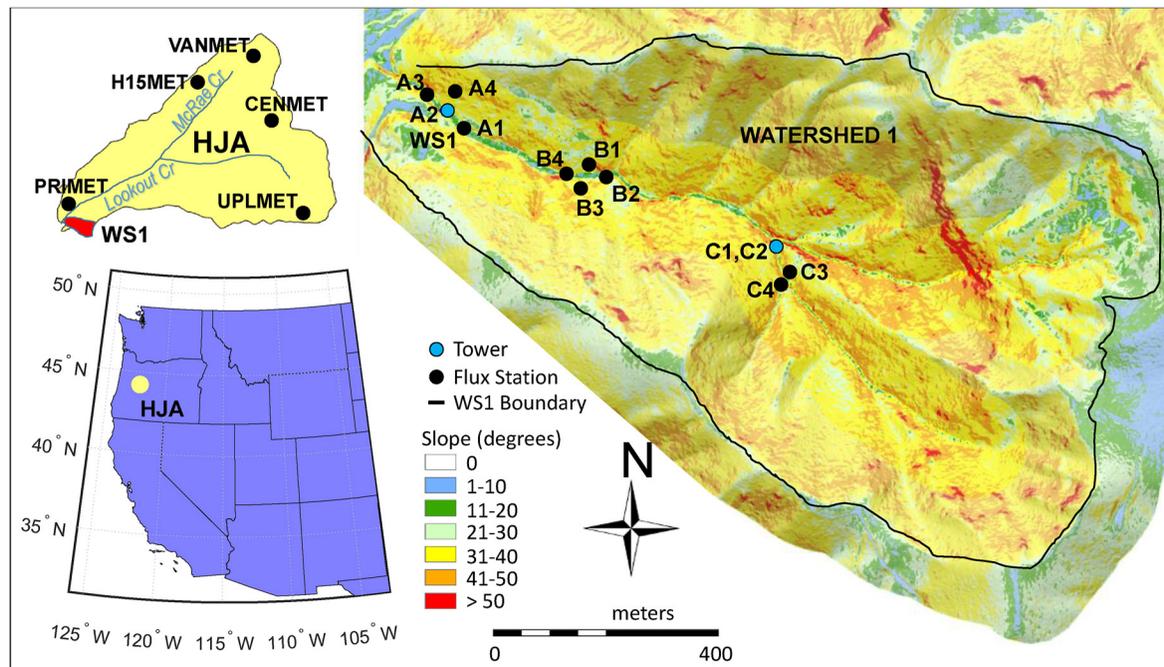
Figure 1. Overview maps show the location of the HJ Andrews Experimental Forest in Oregon, the locations of benchmark stations and the Watershed 1 (WS1) tower within the HJ Andrews domain, and flux station locations within WS1 (source: Theresa Valentine, Corvallis Forest Science Laboratory). The WS1 stream drains into Lookout Creek 150 m below station A3.

Perry & Jones, 2017) (Figure 2). Douglas-fir was planted and aerially seeded during the late 1960s. As of 2012, the planted forest consisted of a dense stand of ~45-year-old Douglas-fir with deciduous red alder (Alnus rubra) along the stream channel. The average height of the canopy was 29 m, and the canopy extended down to 8 m above the ground with understory vegetation from 1 to 4 m high. No thinning has occurred in WS1. Instead, disturbances, such as forest toppling by snow (Lutz & Halpern, 2006) and low-to moderate-severity wildfire in 2020, are modifying forest canopy structure. Many studies in WS1 have examined post-disturbance succession, ecohydrology, carbon budgets, and other topics (e.g., Argerich et al., 2016; Halpern & Franklin, 1990; Hicks et al., 1991; Hood et al., 2006; Moore et al., 2004; Pypker et al., 2007). Basal area, growth rates, and density in the forest plantation in WS1 are within reported ranges for managed and unmanaged forest plantations on steep watersheds in western Oregon (Perry & Jones, 2017).
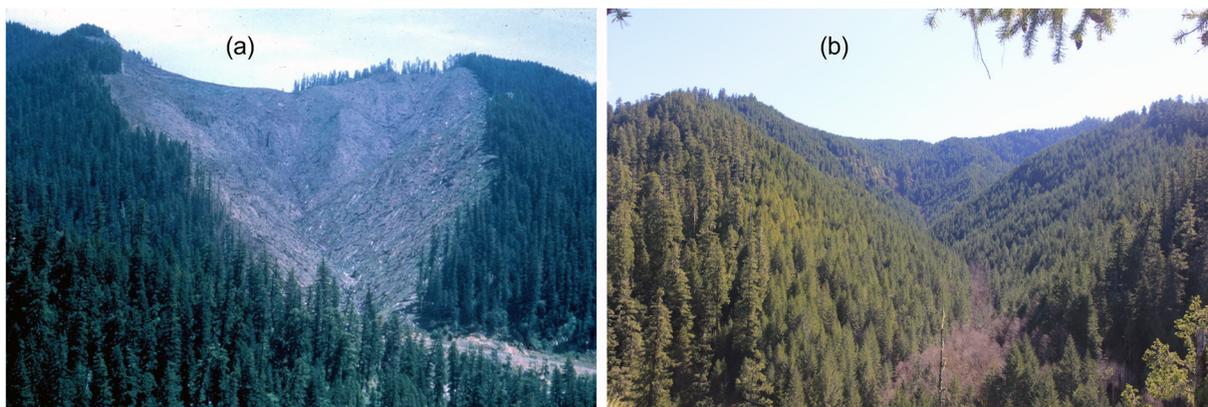

Figure 2. Watershed 1 viewed from the north after clear-cut in the late 1960s (panel a, Photo: Dick Fredricksen) and in 2019 (panel b, Photo: Mark Schulze).

Figure 3. Photographs of example stations. (a) Station A4 was located in a SW-facing canopy opening on a slope of 120 m uphill from the Watershed 1 tower. (b) Station B3 was located on a forested slope and identified by a red ellipse (Photo: Stephen Drake).

2.2. Data Collection

Air flow, heat, and water vapor concentration were measured within three sub-domains along the valley axis (Figure 1). Enclosure-mounted data loggers (Model CR3000, Campbell Scientific Inc. Logan, UT, USA) were deployed at three base sites ranging from 470 to 580 m elevation along a ~1-km transect up the WS1 valley floor from Lookout Creek. At each base site, designated as "A", "B", and "C," data were collected from four stations, labeled, for example, A1, A2, A3, A4, etc. Stations were positioned with the primary goal of measuring subcanopy wind, temperature, and water vapor concentration along the valley axis (stations A1, A2, A3, B2, B4, C1, C2, and C4) and with secondary goals of resolving winds in open locations (station A4) and drainage flow contributions from side slopes (B1 and B3) and tributary channels (C3, Figure 1). Sensors were mounted on tripods at 2-m nominal height above ground level (AGL) and aligned with local gravity. Sensors at sites A2, C1, and C2, were positioned higher above the ground to further resolve bole-space characteristics. Here, "bole-space" is taken as the air volume between the lower fringe of the canopy and the ground. Sensors at A2 were mounted at the 16-m level of a 37-m tower designated as WS1 Tower (Figure 1). Sensors at C1 and C2 were mounted at 7.4 and 12.9 m (boom-extended) on a 12.2-m tower. All A, B, and C sensors were placed below the canopy, except station A4, which was located in a SW-facing canopy opening on a slope 120 m uphill from the WS1 tower (Figure 3a).

Wind speed and direction were sampled at 20 Hz using ultrasonic anemometers (Model Young 81000VRE, RM Young, Traverse City, MI, USA), hereafter referred to as "sonics." Air temperature and humidity were measured using aspirated thermohygrometers (Model Vaisala HMP 155, Vaisala, Finland) paired with each sonic. Thermohygrometers were mounted in actively aspirated radiation shields (Thomas & Smoot, 2013) with inflow at a centroid height of the sonic volume. The thermohygrometers were oversampled at 20 Hz to optimize data acquisition. Wind speed and direction, air temperature, and moisture data obtained in the WS1 watershed were averaged to 1-min intervals.

Additional sensors were mounted on the 37-m WS1 tower in order to determine subcanopy stability and to measure above canopy winds near the watershed outlet. The WS1 tower extended 4 m above the top of the canopy (33 m agl). Temperature was measured using aspirated thermistors (Model 107, Campbell Sci., Logan, UT, USA) mounted at 1, 7, 12, 18, 23, 29, and 37 m, sampled at 10 s intervals and recorded at 1-min averages by a datalogger (Model CR23x, Campbell Scientific, Logan, UT, USA). Tower-mounted instrumentation used in this investigation included open-path CO_2/H_2O analyzers (Model Licor LI-7500, Licor, Lincoln, NE, USA) at 4 and 37 m, an additional sonic anemometer at 4 m (Model CSAT3, Campbell Scientific, Logan, UT, USA), and a 3-axis sonic anemometer at 37 m (Model Gill R2, Gill Instruments, Lymigton, UK) recorded by a datalogger (Model CR3000, Campbell Scientific Ltd. Logan, UT, USA). All tower-based sonic anemometers and open-path CO_2/H_2O analyzers were sampled at 20 Hz.

2.3. Basin-Scale and Regional Reanalysis Data

Basin-scale data of wind speed and direction for the study period were obtained from five HJ Andrews benchmark stations: PRIMET (436 m), H15MET (909 m), CENMET (1028 m), VANMET (1268 m), and UPLMET (1298 m) (Figure 1). Wind speed and direction are measured at 10 m (except for H15MET, which was at 5 m) using propeller anemometers (Model, 05103 Wind Monitor, RM Young, Traverse City, MI, USA). Data were averaged to 15-min intervals. The propeller on this anemometer has a 1 m s^{-1} minimum threshold (Campbell Scientific, Inc, 2015). Sub-1 m s^{-1} averages were kept in subsequent analyses to resolve the diurnal cycle of wind speed with the potential that sub-1 m s^{-1} measurements constituting the 15-min averages may have systematically skewed 15-min wind averages downward during periods with weak winds. The impact of this potential systematic error was minimized by comparing relative changes in wind speed rather than absolute wind speed. Benchmark stations are located in canopy gaps, and the sensor heights are below the surrounding forest canopy, which decreased measured wind speed.

Regional-scale wind data for the study period were obtained from the land component European Centre for Medium-Range Weather Forecasts Re-Analysis 5 (ERA5-Land) (Hersbach et al., 2020; Muñoz-Sabater et al., 2021). This product combines observations and model physics to reproduce hourly atmospheric state variables and derivatives with land surface variables interpolated to grid points with a 0.1° × 0.1° resolution.

From the data collected, spatially distributed and synchronous measurements of temperature, wind speed, barometric pressure, and humidity were available for 50 of the 55 days between July 25 and September 17. Data gaps occurred for three days with the 1 m temperature sensor and for two days with the 4 m sonic anemometer on the WS1 tower. Hereafter, these 50 days are referred to as the 50-day Intensive Observation Period (IPO). In the results and discussion sections, "downslope" refers to down the fall line of a local slope and "downvalley" refers to a direction down the main axis of a valley.

2.4. Data Analysis

To identify the persistence and timing of wind patterns, diel airflow measurements at the WS1 tower were composited (averaged) to highlight features that are commonly observed during the same time daily. Before compositing potential temperature profiles, observed dry-bulb air temperature was converted to potential temperature by correcting for the dry-adiabatic lapse rate of 9.8 K km^{-1}, accounting for temperature differences due to elevation. Individual daily plots were compared with composites to verify that a single, large amplitude anomalous feature on a given day did not unduly bias time composites. No anomalous features were identified and no data were removed as a result of this quality control step. Daily composite data were divided into four distinct time periods based on wind speed and direction following Whiteman (1990) and Pypker et al. (2007). The four time periods are daytime flow (DF), evening transition (ET), nighttime conditions (NC), and morning transition (MT). During clear-sky conditions, the DF time period is distinguished by thermally driven upslope flow above the canopy. The ET time period begins when above-canopy wind direction reverses and air flows downslope. The NC time period begins as turbulence weakens, and NC transitions to the MT as insolation initiates upslope flow above the canopy the following morning.

The strength and effects of the subcanopy inversions created by heating of the forest canopy were examined by calculating static stability, wind speed, and latent heat flux during DF at the WS1 tower for the 50-day IOP. Maximum subcanopy static stability (Stull, 2012) was computed during the time period of peak canopy heating (13:30 to 14:30, local time). Static stability was computed as the average potential temperature difference between the 1 and 23 m heights on the WS1 tower divided by the difference in height (K m^{-1}). Static stability is used as a measure of subcanopy stability rather than the stability parameter used in Wang et al. (2015) because the Obukhov length is not a valid stability parameter within the roughness sublayer (Vickers & Thomas, 2014) or for katabatic flow (Oldroyd et al., 2016). Bole-space wind speed and direction were calculated at 4 m height on the WS1 tower for the same 13:30 to 14:30 time frame as static stability. Wind direction was classified into two categories: variable (all directions) and downvalley, defined as wind direction ±25° within the most prominent downvalley direction. During periods of variable winds, even if the wind has a downvalley component, intermittent turbulence and coherent structures in above-canopy winds may have significantly influenced the subcanopy

wind direction during discrete events. These one-hour averages of static stability, wind speed, and wind direction variability were used to characterize wind regimes as a function of subcanopy static stability.

Turbulence kinetic energy (TKE) is the kinetic energy, usually expressed per unit mass, associated with eddies in a turbulent flow. TKE in the subcanopy drives the vertical exchange of moisture across the boundary from the forest canopy to the air above. Thirty-minute-averaged TKE was calculated for each station as (Stull, 2012)

$$\frac{\text{TKE}}{m} = 0.5 \left(\overline{u'^2} + \overline{v'^2} + \overline{w'^2} \right) \tag{1}$$

where m is mass, u', v', and w' are instantaneous deviations from 30-min mean wind components and the overbar represents a 30-min average. TKE was calculated for subcanopy stations at the 2-m nominal height of the sonic anemometers.

Turbulence intensity (TI) is defined as the standard deviation of wind speed, σ_M, divided by the mean wind speed, $\overline{M}$ (Stull, 2012):

$$\text{TI} = \frac{\sigma_M}{\overline{M}} \tag{2}$$

and provides a normalized measure of turbulence.

To assess the relationship of subcanopy dynamics in WS1 to the basin and the region, wind speed data from benchmark stations PRIMET (430 m elevation), H15MET (909 m), CENMET (1020 m), VANMET (1275m), and UPLMET (1295 m) throughout HJ Andrews (Figure 1) were averaged for each day of the study period.

To assess the effect of subcanopy inversions and winds on moisture fluxes within and through the forest canopy, the difference in water vapor concentration in the subcanopy compared with the air above the canopy was determined as water vapor concentration (mol m^{-3}) at 4 m minus the water vapor concentration at 37 m, integrated over the DF period, for each day of the study period, and this was related to the maximum static stability on each day.

To test the hypothetical effect of climate warming on subcanopy winds and moisture transport, we calculated wind speed and virtual temperature differences between stations B4 and C4 along the main channel for days with relatively high subcanopy stability and determined the relationship between these air temperatures and wind speed differences between these two sites. We then used this relationship to determine the effect of a 0.1 K m^{-1} increase in static stability on downslope water vapor transport by subcanopy winds. As in prior studies from this site (i.e., Pypker et al., 2007), downslope moisture transport is computed at the airshed exit although localized moisture fluxes are also present within the watershed boundary where moisture gradients are present.

3. Results

Above and subcanopy wind speed and direction are composited for the experimental period in Sections 3.1 and 3.2 to summarize the local wind patterns. Winds are then categorized into four daily time periods (Section 3.3). We examine how inversion strength (static stability) is related to wind speed and how turbulence and latent heat flux varies over the day, above, and below the canopy, for low-stability and high-stability conditions (Section 3.4). We show that on days with high static stability, the downslope subcanopy wind speed increases with stability, and low-stability days are associated with higher TI but lower temperature below the canopy (Section 3.5). The coherence of subcanopy wind and above-canopy winds within the larger Lookout Creek basin is investigated in Section 3.6. In Section 3.7, results indicate that stronger subcanopy inversions are associated with greater subcanopy humidity, relative to the air above the canopy, and these stronger subcanopy inversions (on high-stability days) constrain subcanopy mixing and vertical moisture flux out of the canopy relative to low-stability days. Finally, we use the relationship of wind speed and virtual temperature differences between stations B4 and C4 along the main channel for high-stability days to test the systematic effect of canopy warming on subcanopy winds and moisture transport (Section 3.8).
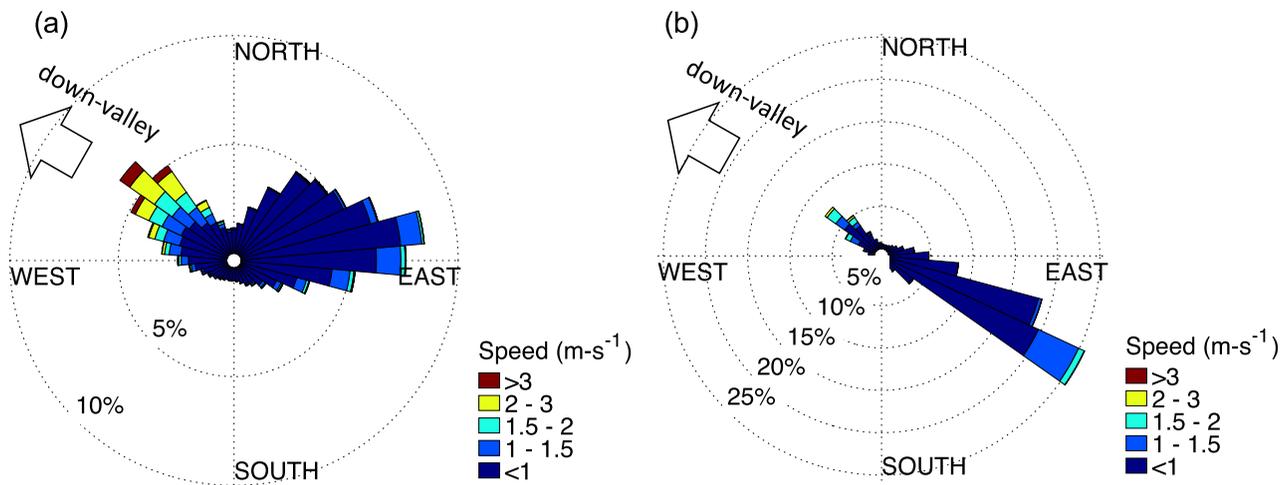
Figure 4. Windroses on Watershed 1 tower color-coded by wind speed at 37 m above ground level (AGL) (above canopy, panel a) and at 4 m AGL (below canopy, panel b).

Summer and fall seasons in the PNW are typically dry, dominated by a persistent high-pressure synoptic pattern. However, June 2012 antecedent conditions in the HJ Andrews region were very moist with a Palmer Z index between 2.5 and 3.5 (NOAA NCDC Annual Drought Report, 2012, see also supplement section S1). During the study period (19 July 2012 to 17 September 2012), Oregon ranked as the second driest state and much of the continental USA experienced drought conditions throughout this time period. Consequently, the progressive decrease in latent heat flux between the beginning of July and end of September was representative for a drought index transition from very moist to severe drought conditions. The prolonged dry period during the study period provided favorable conditions for isolating the effects of subcanopy stability on moisture transport.

3.1. Above Versus Below-Canopy Winds

Based on 1-min averaged data acquired from July 25 to 17 September 2012, wind above the canopy at WS1 tower had two prominent directions: from the NW and from the ENE (Figure 4a). The strongest winds were from the NW due predominantly to upvalley DF and topographic steering rather than synoptic forcing at this locale (see also Figure S2 in Supporting Information S1 with overview of synoptic forcing in the supplement). Above the canopy, weaker downvalley (Lookout Basin) and downslope winds from the eastern portion of the WS1 basin were common during nighttime throughout the study period. Wind above the canopy was more variable than below the canopy, in part due to three-dimensional vorticity of turbulent eddies at the time scale of 1-min averages that is greater above the canopy than below it. In contrast, wind direction below the canopy at 4-m height was bimodal, aligning with the watershed axis (Figure 4b). Subcanopy wind direction along the valley axis was primarily downvalley throughout the day (Figure 4b). The consistently lower speed and more directional winds at 4 m compared to 37 m indicate that the canopy acts as a permeable mechanical and thermodynamic barrier that dampens through-canopy turbulent fluxes.

3.2. Wind Patterns as a Function of Canopy Cover and Position Within the Watershed

Below the canopy (2 m), downslope winds occurred throughout the watershed during both daytime and nighttime. The relative frequency of downslope flow varied by position in the watershed and by canopy cover (Figure 5). Below-canopy winds were primarily downvalley throughout the day at sites located along the axes of tributaries in the upper valley (C2, C3, and C4) and at sites aligned with the channel axis in the mid-valley (B2 and B4). In contrast, below-canopy wind direction was primarily downslope at sites positioned slightly higher above the valley axis (B1 and B3); these sites were dominated by downslope rather than downvalley flow because they were positioned generally above the depth of downvalley cold air drainage flows. In addition, wind direction was quite variable at a location having a canopy opening (site A4, Figures 3a and 5); this site was exposed to above-canopy
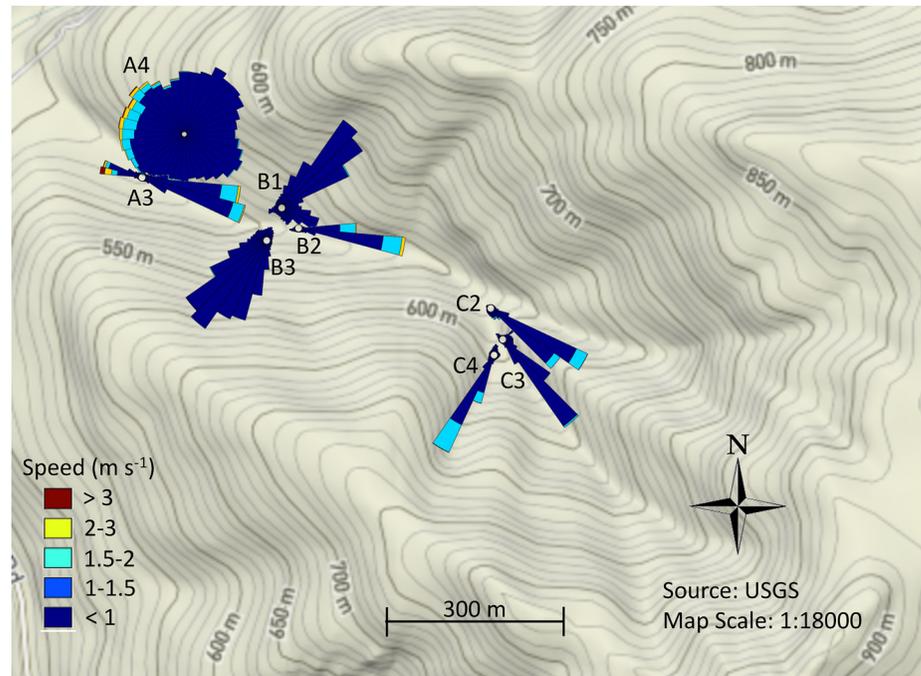
Figure 5. Windroses of 1-min averaged winds at 2 m nominal height for subcanopy stations A3, A4, B1, B2, B3, C2, C3, and C4 in Watershed 1. Stations A1 and B4 have very similar windrose shapes as station A3 in Figure 5 but are not rendered to avoid overlapping. Windrose bin sizes are rescaled to avoid overlap and highlight features described in the text (Map source: USGS).

winds, multiscale forcing, edge effects, and turbulence, which disrupt the nocturnal/downslope, daytime/upslope wind regime.

3.3. Four Time Periods of Wind

Average wind speed and direction at the WS1 tower clearly display four time periods of: MT, DF, ET, and NC (Figure 6a). After the MT, wind speed above and below the canopy increases during the DF period and gradually diminishes throughout the NC period. During the MT, solar heating in Lookout Creek Basin erodes the cold air pool and subcanopy gravity-driven flow increases following a brief weak wind direction reversal (Figure 6b). This subcanopy MT wind reversal is likely caused by a pressure gradient adjustment during the transition from the NC to DF period and is a characteristic of transition periods in mountainous regions (Nadeau et al., 2012, 2018). Above the canopy, downslope winds exhibit a local maximum in magnitude during MT (Figure 6a) as solar heating in Lookout Creek Basin initiates a mountain breeze that precedes solar heating in the WS1 basin (see also Section 3.6). As given by a linear regression, the time of maximum wind speed at 37 m agl was 19 min earlier in the day at the end of the IOP relative to the beginning of the IOP. With decreasing daylength during the IOP, the maximum wind speed at 37 m height was thus achieved with 80 fewer daylight minutes at the end of the IOP relative to the beginning of the IOP.

The ensemble maximum inversion (5.6°C difference in temperature at 37 vs. 1 m) occurred at 14:46, consistent with canopy heating by solar insolation (Figure 6c). During DF (DT), the subcanopy wind speed peaks at 14:36 about 10 min before the time of maximum temperature inversion within the canopy, whereas the above-canopy wind speed peaks at 15:15 about 29 min after the time of maximum inversion (Figures 6a and 6c). As given by a linear regression, the time of maximum air temperature at 37 m agl was 14 min earlier in the day at the end of the IOP relative to the beginning of the IOP. With decreasing daylength during the IOP, the time of maximum air temperature was thus achieved with 75 fewer daylight minutes at the end of the IOP relative to the beginning of the IOP. During the ET, wind directions roughly align above and below the canopy as nocturnal drainage flow reestablishes above the canopy. Gravity flow decreases throughout the night as nocturnal drainage flow fills the valley with cold air until the MT and the diurnal cycle repeats. In Figures 6a–6c, sunrise, solar noon, and sunset
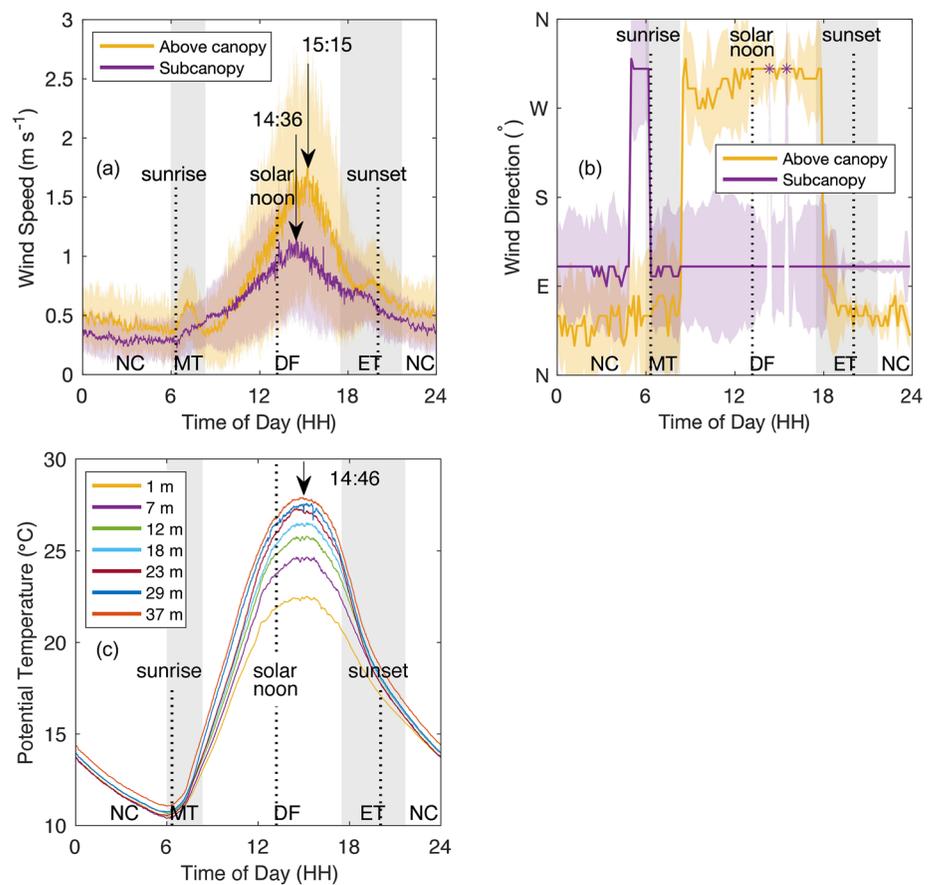
Figure 6. Composite wind speed (a), wind direction (b), and potential temperature for heights ranging from 1 to 37 m (c) at the Watershed 1 (WS1) tower for the period 19 July 2012 to 17 September 2012, and four flow regimes (vertical white and gray bars): daytime flow, evening transition, nighttime conditions, and morning transition. Flow regimes are defined as in Whiteman (1990) and Pypker et al. (2007). Wind speed is shown above the canopy at 37 m (gold) and below the canopy 4 m (purple) (panel a) with time of peak winds delineated by arrows. Composite wind directions are defined by the mode of wind direction at each minute in 10-degree bins (panel b). Shading indicates one standard deviation. Purple asterisks in panel (b) indicate two short time periods when the subcanopy wind direction mode at the WS1 tower was preferentially upvalley.

were obtained from the NOAA/ESRL calculator (Cornwall et al., 2014) for 21 August 2012, the midpoint of the IOP.

The subcanopy diurnal wind direction response in the WS1 basin (Figures 5 and 6) is different from the archetypal mountain breeze regime. An archetypal, thermally driven mountain breeze presents upslope flow during the DF period that increases with increased heating (Schmidli, 2013). In contrast, along the valley axis, the dominant subcanopy wind direction was downvalley (Figure 5), and the highest subcanopy wind speeds were downvalley at representative stations along the valley axis (Figures 6a and 6b). These differences appear to be due to the presence of an even-aged dense forest canopy, which creates an inversion that modulates below-canopy air flows.

3.4. Daytime Flow Mode

Over the 50-day IOP, the relationship of 4 m subcanopy wind speed to static stability differs below and above a stability transition zone (gray bar in Figure 7a). For days with static stability values below 0.17 K m^{-1}, wind speed is not correlated with stability (red data points, $R^2 = 0.04$). For days with static stability values above 0.21 K m^{-1}, downvalley wind speed increases with increasing static stability (blue data points, $R^2 = 0.42$). Other factors, such as the coherence of diel pressure gradient evolution and shortwave solar insolation, also influence wind speed (Figures S3 and S4 in Supporting Information S1).
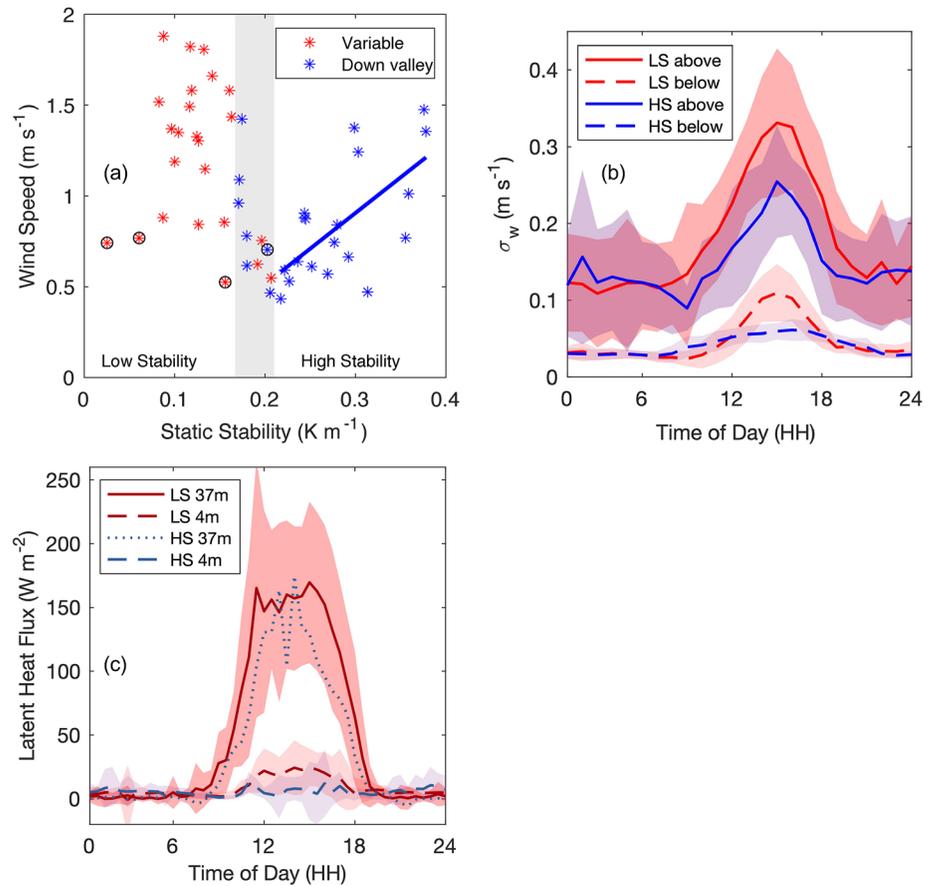
Figure 7. Relationship of composite 4 m wind speed to static stability (a); composite σ_w over the day (b), and composite latent heat flux over the day (c). Panel (a) shows Watershed 1 tower 4-m mean wind speed versus canopy static stability over the 1- to 23-m layer during the time period 13:30 to 14:30 for each of the 50-day IOP. Wind speed is coded by dominant daily wind direction (variable = red or downvalley = blue). Overcast days are circled. (b) Composite standard deviation of the vertical wind speed component by time of day computed at 37 m (above canopy) and 4 m (below canopy) heights for low static stability (LS) and high static stability (HS) days indicated in panel (a). (c) Composite latent heat flux at 4-m and 37 m heights for LS and HS days. Shading in panels (b) and (c) represent $\pm$ one standard deviation from the composite.

The standard deviation of vertical wind speed, σ_w, was greater during low-stability days compared with high-stability days, both above and below the canopy (Figure 7b), indicating greater potential for vertical mixing on low-stability days. The standard deviation of vertical wind speed was many times higher above than below the top of the canopy. Below the canopy, the low-stability maximum σ_w ($\sim$0.1 m s^{-1}) was twice the high-stability value ($\sim$0.05 m s^{-1}), while above the canopy, the low-stability maximum σ_w (0.33 m s^{-1}) was 33% greater than the high-stability value (0.25 m s^{-1}). These findings, combined with the relationship of wind speed to stability (Figure 7a), indicate that subcanopy mixing was suppressed on high-stability days relative to low-stability days. The likely physical mechanism for this σ_w reduction is the enhanced temperature inversion on high-stability days, because the buoyancy restoration force has larger magnitudes in stably stratified fluids (Vickers & Thomas, 2013).

These effects on vertical mixing produce much higher latent heat fluxes just above the canopy compared to below the canopy, and 26% greater vertical moisture loss via mixing during low-stability days compared to high-stability days just above the canopy (37 m) (Figure 7c). Latent heat fluxes were computed by eddy covariance with the UtahEFD/UTESpac flux package as in Jensen et al. (2016). But for brief spikes at 13:00–15:00 on high-stability days, the ensemble latent heat flux at 37 m was higher throughout the DF period during low-stability days compared with high-stability days, indicating more continuous through-canopy mixing on low-stability compared with high-stability days. Latent heat fluxes above the canopy on high-stability days were highly variable with a standard deviation that spanned the full range in Figure 7c. Therefore, standard deviation is not rendered in Figure 7c for HS days and the above-canopy composite is displayed as a dotted line to signify high variability.
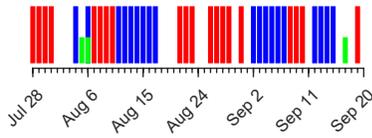
Figure 8. Days in the 50-day IOP classified as low-stability (red) or high-stability (blue) based on the analysis in Figure 7a. Days with precipitation are shown in green.

The finding of distinctly different DF flow regimes permits classifying days in the 50-day IOP according to their DF values of static stability and associated moisture flux characteristics (Figure 8). Twenty-one of the 50 days were low stability, 19 were characterized as high stability, and 10 days were transitional. In this context, "low-stability" still represents some degree of stability in the subcanopy lapse rate and should not be confused with an unstable (convective) lapse rate. Low- and high-stability periods tend to persist for several consecutive days.

Atmospheric conditions that differentiate low-stability from high-stability days are examined in the supplement. A distinguishing characteristic of HS days is synchronicity of the pressure tendency that is lacking on LS days. As will be shown in Section 3.6, the basin-wide, daytime change in wind speed is smaller on HS days relative to LS days.

3.5. Along-Valley Wind Characteristics

Subcanopy wind speed during daylight hours in the July 25 to September 17 study period was consistently higher on high-stability days than on low-stability days at the three stations along the WS1 valley axis (A1, B4, and C4) (Figure 9a). For each of the three instrumented areas along the watershed axis, these three subcanopy stations (A1, B4, and C4) were most representative of their respective locations for the following reasons: (a) station A3 was closer to the watershed outlet than A1 so it was more subjected to dynamics within the greater Lookout Creek
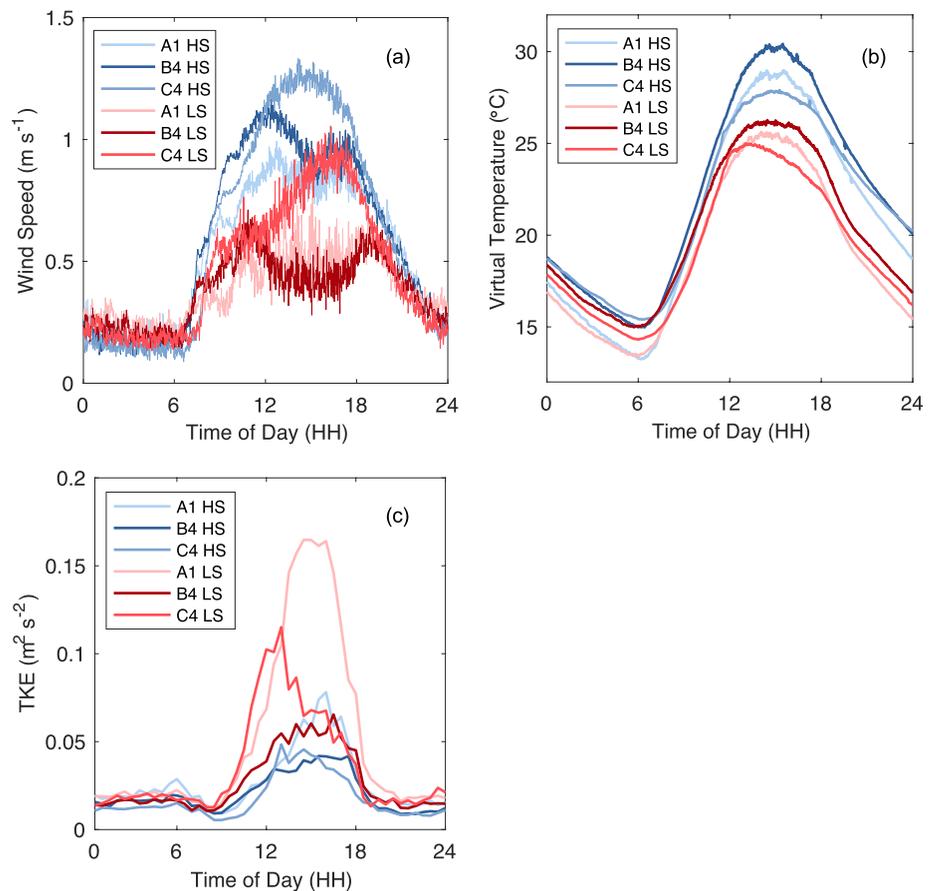

Figure 9. Comparison of subcanopy wind speed during high static stability (HS) and low static stability (LS) days at selected stations in Watershed 1 (panel a). In panel (b), subcanopy 1-min averaged virtual temperatures and in panel (c) 30-min averaged Turbulence kinetic energy are compared at the same stations as in panels (a) and (b) for HS and LS days. All measurements were obtained at 2-m nominal height agl.

basin; (b) station B2 was subjected to stronger downslope flow from side slopes than B4; and (c) station C3 was surrounded by denser undergrowth than C4.

Subcanopy wind speed was more variable during LS days (shades of red in Figure 9a) than HS days. Composite virtual temperature (T_v) was greater on HS compared with LS days at stations A1, B4, and C4 (Figure 9b). Lower subcanopy T_v during LS days compared with HS days may be the result of a weaker inversion and greater prevalence of large, coherent eddies on LS days that inject relatively dry above-canopy air into the subcanopy. Several overcast days (Figure 7a, Figure S4 in Supporting Information S1) also contributed to lower ensemble subcanopy T_v during LS days.

During the afternoon on HS days, air at station C4 (an upstream tributary) was denser (had a lower T_v) than at B4 or A1 (in the main channel) (Figure 9b). Denser air increased katabatic acceleration at C4 relative to B4 or A1, producing the higher wind speed observed at C4 compared with A1 or B4 (Figure 9a). Even for LS days, a katabatic signature was evident at station C4 where increased afternoon cooling relative to stations A1 and B4 was associated with an increase in afternoon wind speed (Figures 9a and 9b). On the other hand, on HS days, T_v and wind speed at midday were higher at B4 (axis of main channel, midway down the valley) than A1 (axis of main channel, near mouth of the watershed), counter to the density effect on katabatic acceleration. This discrepancy could be attributed to mass continuity and the widening of the valley floor at A1, which increases subcanopy volume, thereby slowing subcanopy winds. Differences in subcanopy roughness and canopy elements between stations also may be a contributing factor in the observed differences in subcanopy wind speed (Thomas, 2011) despite efforts to locate stations to minimize along-slope flow disruption by vegetation.

TKE was higher during daylight hours, higher on low-stability compared to high-stability days, and higher at stations A1 (valley mouth) and C4 (upper valley) than B4 (midway down the valley) (Figure 9c). Station B4 had relatively low TKE on both LS and HS days, whereas station A1 exhibited the highest TKE for all days. As before, high variability in wind speed and enhanced TKE generation can be attributed to proximity of station A1 to the WS1 airshed outlet to Lookout Creek. Relatively low subcanopy wind speeds (Figure 9a) coincided with relatively high TKE on LS days at A1, and the highest average composite wind speed coincided with the lowest average composited TKE at 1500–1800hr on HS days at station C4 (Figure 9c). While increased wind speeds, which at these subcanopy sites occur with the HS condition, are typically related to high shear generation, higher stability likely suppresses vertical TKE transport across the canopy. This result is consistent with Figure 7b, which showed that on LS days, above-canopy winds ventilate the subcanopy and large eddies introduce TKE into the subcanopy environment. Below the canopy, vertical mixing is enhanced along the valley axis on LS days and suppressed on HS days.

3.6. Basin-Scale Wind Patterns

In this section, basin-scale winds measured by benchmark stations across the HJ Andrews Experimental Forest are compared with ERA5-Land simulated winds at one grid point within the HJ Andrews boundary. Wind speed during the study period increased with elevation and ERA5-Land modeled wind speed was approximately two times greater than wind speed measured by the benchmark stations at 10-m height (Figure 10a). This result is unsurprising because of poor model resolution of simulated orography and canopy effects. Daily averaged wind speeds for stations over the period of the study were similar on HS versus LS days at elevations ranging from 436 to 1298 m and from ERA5-Land (Figure 10a), given by close proximity of data markers to the 1-to-1 diagonal. The error bars showing ±1 standard deviation in Figure 10a indicate that variability in measured wind speed for benchmark stations was greater for LS days compared to HS days, consistent with subcanopy measurements in WS1 (Figures 7a and 9a). This difference in wind speed variability, however, was not captured by the ERA5-Land analyses. Midday wind direction for all stations (not shown) was upvalley indicating that differential insolation on topography drives basin-scale windflow above the forest canopy for both LS and HS days. On days classified as low-stability, on average, wind speed increased more from 6 a.m. to the maximum wind speed in the afternoon, both at benchmark stations in canopy gaps and in the ERA5-Land reanalysis, compared to high-stability days (Figure 10b). This result indicates that above-canopy mountain breezes accelerated more during LS days. Stronger acceleration of above-canopy winds and increased TKE on LS days relative to HS days moderates solar heating of the canopy and limits development of a subcanopy inversion and downvalley subcanopy winds (Figure 7).
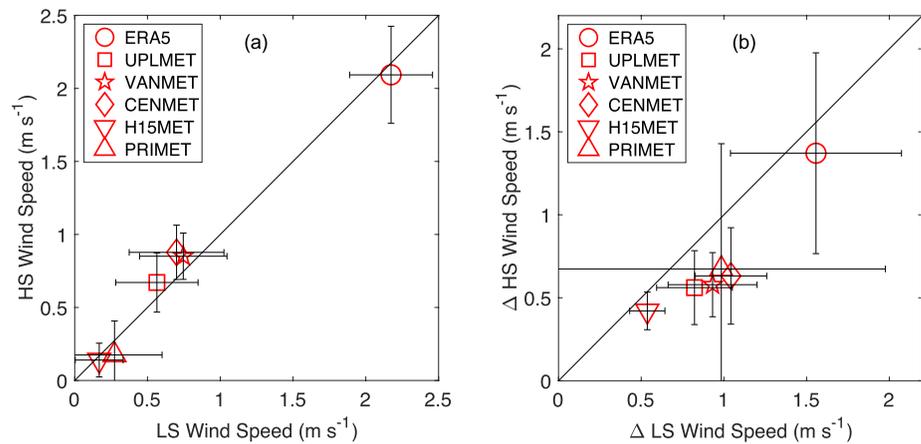
Figure 10. Relationship of average wind speed on high-stability days versus low-stability days in the study period (19 July 2012 to 17 September 2012). (a) Average daily wind speed for high static stability and low static stability days, (b) average daily increase in wind speed from 6 a.m. PST until the afternoon wind speed maximum from ERA5-Land (10-m winds) and at benchmark stations. Vertical and horizontal bars indicate one standard deviation, determined independently for each axis.

ERA5-Land pressure gradient and 10-m wind speed provide more support for increased mountain breeze development during LS days. The 00Z (16:00 PST) ERA5-Land surface pressure gradient averaged 2.5% greater on LS days versus HS days for the basin average. Since ERA5-Land gridded products represent averaged quantities for a given grid box, the actual pressure gradient difference over smaller, localized scales likely exceeds this value. An increased horizontal pressure gradient on LS days over the HJ Andrews region favored accelerating above-canopy wind speed and turbulence that would ventilate the canopy, decreasing thermal stratification through the canopy relative to HS days.

Collectively, these results illustrate that ERA5-Land products do not capture subcanopy wind state and do not accurately resolve above-canopy wind speed or wind speed variability for this region. However, ERA5-Land wind and pressure products have some skill for capturing wind and pressure tendencies that can be used to discriminate LS from HS days. For the benchmark stations and ERA5-Land analyses, low-stability days corresponded to days when above-canopy upslope winds directly influenced subcanopy winds. During days with high subcanopy stability, above-canopy winds tended to remain decorrelated from subcanopy winds throughout the DF period.

3.7. Moisture Gradients and Fluxes

The difference in daily composited water vapor concentration between 4 and 37 m reached its maximum during the DF period on high-stability days (Figure 11a). The gradient of virtual potential temperature, which already accounts for the water vapor influence on buoyancy, was 47% less than the potential temperature gradient between 4 and 37 m agl at the WS1 tower. So greater subcanopy moisture decreased static stability but not enough to erode the stable layer. Because total precipitation was low (31 mm) and infrequent (spread over 3 days) during the study period (Figure 8), short-term differences in vadose zone water available for evaporation or transpiration between HS and LS days were unlikely to account for the observed difference in water vapor concentrations above and below the canopy.

The difference in water vapor concentration between the generally moister subcanopy and drier above-canopy air increased with subcanopy static stability (Figure 11b; $R^2 = 0.67$). In other words, stronger subcanopy inversions are associated with greater humidity, relative to the air above the canopy. Lower latent heat flux on HS days relative to LS days both above and below the canopy (Figure 7c) as well as lower subcanopy TKE implies that stronger subcanopy inversions on HS days constrain mixing and vertical moisture flux out of the canopy. As vertical mixing is more constrained, subcanopy moisture concentration increases and, for a given downslope wind speed, more moisture is advected downslope by subcanopy winds.
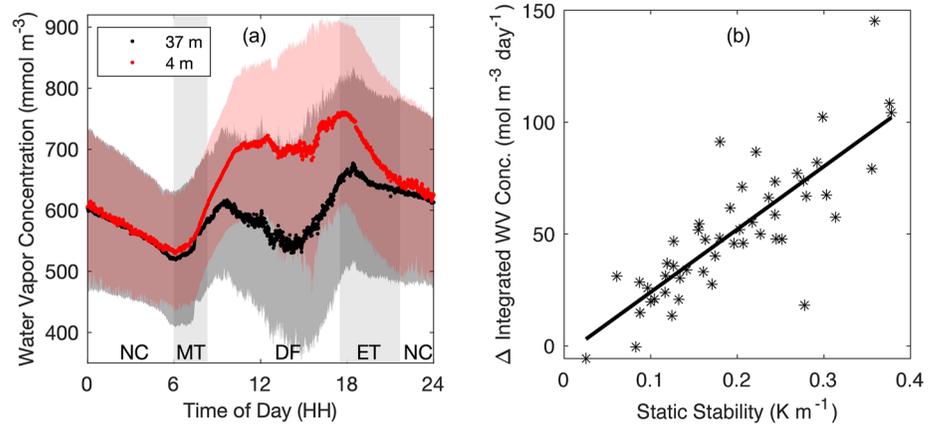
Figure 11. Relationship of water vapor concentration to static stability. (a) Composited water vapor concentration over time during the day for high-stability days at 4 m (red) and 37 m (black). (b) Difference in average daily water vapor concentration, 4 m minus 37 m, versus the daily maximum stability (1 hr averaged) for all days in the study period.

3.8. Wind Speed and Potential Temperature Along the Watershed Axis

The difference in subcanopy wind speed was positively related to the difference in air temperature between the two along-channel stations (B4 and C4) for HS days in the 50-day IOP ($R^2 = 0.47$). The slope of the relationship suggests that a 1 m s^{-1} increase in wind speed corresponds to a 3°C increase in T_v between these two stations. An increase of 0.1 K m^{-1} in static stability for the 12:30–13:30 hr period on high-stability days is associated with a 0.3 m s^{-1} increase in wind speed (Figure 7a), which in turn corresponds with a 1K increase T_v between B4 and C4, well within the range measured during this experiment. Since subcanopy wind speed (Figure 7a) and water vapor concentration (Figure 11b) both increase with increasing stability, an increase in static stability produces a positive feedback of water vapor advection through the subcanopy space. For example, a 0.1 K m^{-1} increase in dry-static stability produces a 17% diagnosed increase in water vapor transport by downslope winds relative to the observations (see also the supplement, Section S5).

4. Discussion

The presented results document a flow regime within a PNW coniferous forest that adjusts to the relative intensity of subcanopy static stability. Wind above the canopy can more easily mix with subcanopy air on days when subcanopy stability is low, thereby producing larger latent heat fluxes through the canopy than on days when subcanopy stability is greater. In contrast, strong subcanopy stability restrains vertical moisture flux and engenders increased subcanopy humidity and increased downslope moisture advection. To the authors' knowledge, these linkages between subcanopy stability and vertical versus downslope vapor transport are a novel finding for forested regions. A linear cause and effect paradigm does not fully describe the development of LS versus HS days because, for example, greater through-canopy mixing weakens stability, which further promotes vertical moisture flux, reinforcing an LS condition. On HS days, increased downslope moisture advection in a plantation forest changes the distribution of moisture relative to LS days in this even-aged conifer forest. The findings reported in this study may provide a mechanism to explain why summertime evapotranspiration in uniformly structured conifer plantations may exceed that of more complex canopies of native forests.

Comparing the results of this study with previous studies, the strongest subcanopy downslope winds occurred under the highest stability conditions. However, Wang et al. (2015) found the strongest downvalley winds during moderate stability regimes in a temperate, deciduous forest valley (Wang et al., 2015). Differences in slope and forest canopy structure in this study likely account for different findings compared to Wang et al. (2015). For example, Moon et al. (2019) and Thomas (2011) found large variability in subcanopy wind speed profiles and other statistics caused by variations in canopy structure. Valley configuration (width and depth) also affects the strength of downslope flow and resulting development of a cold air pool (Kiefer & Zhong, 2015). In unvegetated mountains, under high-pressure conditions typical of summer in the PNW of the USA, local winds convey heat and water vapor upslope during the day, but downslope at night (e.g., Geiger et al., 2009; Oke, 2002).

However, the results of this study show that under high-pressure conditions, the presence of a forest canopy creates a subcanopy inversion, which strengthens the buoyancy force that drives flow down the slope and enables downslope winds to persist for much of the daytime. TKE and latent heat flux profiles for LS days (Figure 7b) are indicative of above-canopy coherent structures that disturb the subcanopy air space and promote the loss of subcanopy moisture (Finnigan, 1979; Shaw et al., 1983; Thomas et al., 2008). Factors affecting moisture fluxes in forests are complex and not all moisture sources and sinks were quantified in this study. Soil conditions and physiological processes, such as the influence of stomatal conductance on evapotranspiration, though not included in this investigation, merit inclusion in future studies of subcanopy moisture advection.

When considering broader implications of the observations detailed in this study, we acknowledge that regional climate models (RCMs) do not resolve the subcanopy wind regime. However, RCMs have skill to predict how climate forcings may change under different climate scenarios and thereby influence subcanopy moisture transport processes. The regional climate model ($\sim$25-km resolution) runs under Representative Concentration Pathway 4.5 project an increasing summer/autumn 500 mb high-pressure anomaly in the PNW relative to areas outside of the western US (Rupp et al., 2017). Summer precipitation has been declining since 1980 based on USHCN records for Oregon and Washington (Menne et al., 2009) and is expected to continue to decrease (Rupp et al., 2017). These trends will increase air temperature and reduce relative humidity above the canopy during the summer, decreasing surface latent heat flux while increasing sensible heat flux from PNW forests. Increases in the ratio of sensible heat flux to latent heat flux (Bowen ratio) increase the strength of mountain breezes (Alpert & Mandel, 1986; De Ridder & Gallée, 1998). Therefore, the increased sensible heat flux over PNW forests predicted by Rupp et al. (2017) would be due not only to energy repartitioning from latent to sensible heat (which is resolvable by an RCM) but also due to increased subcanopy mixing as a consequence of increased surface layer wind speed (which is not resolvable by an RCM). This finding implies that regional climate warming over PNW forests will reduce subcanopy moisture, potentially limiting moisture-mediated microclimate refugia in these seasonally dry conifer forests (e.g., Davis et al., 2019).

Treating sensible heat flux as an independent variable, increased diabatic heating on a PNW coniferous forest should increase the strength of the mountain breeze on LS days. However, interdependencies of environmental variables and feedbacks between them are not fully understood so we also consider the possibility that winds at canopy level weaken, allowing a strengthened subcanopy inversion. The physical rationale for considering this alternative is that regionally predicted lower relative humidity may increase partitioning of solar insolation into sensible heat, leading to increased warming at canopy level and thereby strengthening the subcanopy inversion on days when above canopy winds do not significantly increase. One can diagnose the increase in wind speed and water vapor concentration as static stability increases on HS days from the slope of the regression that relates wind speed to dry-static stability on HS days (Figure 7a) and the slope of the regression that relates water vapor concentration to dry-static stability (Figure 11b). Combining these equations allows one to estimate the increase in downslope water vapor transport as static stability increases on HS days. In summary, RCM trends support increasing evaporative demand for the forest canopy on days with low subcanopy stability and increasing downslope advective flux on days with high subcanopy stability.

5. Conclusions

In this intensive field study in a 45-year-old conifer plantation in a steep mountain valley in Oregon, USA, heating of the forest canopy produced subcanopy inversions, whose strength regulated a bimodal wind regime during the dry season. On days with relatively weak canopy heating and relatively weaker subcanopy temperature inversions, above canopy winds more efficiently exchange subcanopy air, leading to greater than average vertical moisture flux and weaker than average along-slope, subcanopy water vapor advection. On days with relatively strong canopy heating and stronger subcanopy temperature inversion, vertical moisture flux is suppressed and daytime downslope winds are stronger than average under the canopy. Increased downslope advection redistributes subcanopy water vapor and other atmospheric constituents from upslope to downslope areas, providing an alternate method of drying the subcanopy environment that is not resolved in regional models. Regional-scale increases in Bowen ratio predicted by a regional climate model suggest that both vertical and horizontal water vapor transport from the forest will be enhanced as the climate warms. These findings have implications for how plantation forests respond to climate change.

The key finding of this study—a uniform canopy structure favors a subcanopy wind regime that transports moisture out of the watershed—may be relevant to forest water use and climate change over much larger areas. Steep plantation watersheds such WS1 are individually small but in aggregate occupy an ecologically significant percentage of the land area in the PNW. The forest canopy structure and landform setting of WS1, and hence the results of this study, are representative of intensively managed, even-aged, uniformly structured forest plantations on mountainous private industrial forest lands. Further work is needed to examine how forest canopy structure and subcanopy wind regimes influence vegetation-atmosphere interactions and moisture dynamics.

Data Availability Statement

Benchmark station data (Daly & McKee, 2019) are available as data set MS001 through the Andrews Data Catalog and served by the EDI Data Portal via (DOI: https://doi.org/10.6073/pasta/c021a2ebf1f91adf0ba3b5e53189c84f). IOP station data Thomas (2017) are available as data set MV007 through the Andrews Data Catalog and served by the EDI Data Portal via (DOI: https://doi.org/10.6073/pasta/e1dcac713961e62c3aaad2816bbf7780).

References

Alpert, P., & Mandel, M. (1986). Wind variability—An indicator for a mesoclimatic change in Israel. *Journal of Applied Meteorology and Climatology*, *25*(11), 1568–1576. https://doi.org/10.1175/1520-0450(1986)025<1568:WVIFAM>2.0.CO;2

Argerich, A., Haggerty, R., Johnson, S. L., Wondzell, S. M., Dosch, N., Corson-Rikert, H., et al. (2016). Comprehensive multiyear carbon budget of a temperate headwater stream. *Journal of Geophysical Research-Biogeosciences*, *121*(5), 1306–1315. https://doi.org/10.1002/2015JG003050

Brutsaert, W., & Parlange, M. B. (1992). The unstable surface layer above forest: Regional evaporation and heat flux. *Water Resources Research*, *28*(12), 3129–3134. https://doi.org/10.1029/92WR01860

Campbell Scientific, Inc. (2015). *RM Young wind monitor instruction manual*.

Cornwall, C., Horiuchi, A., & Lehman, C. (2014). *NOAA ESRL sunrise/sunset calculator*. Retrieved from https://gml.noaa.gov/grad/solcalc/sunrise.html

Daly, C., Conklin, D. R., & Unsworth, M. H. (2010). Local atmospheric decoupling in complex topography alters climate change impacts. *International Journal of Climatology*, *30*(12), 1857–1864. https://doi.org/10.1002/joc.2007

Daly, C., & McKee, W. (2019). Meteorological data from benchmark stations at the Andrews experimental forest, 1957 to present. Corvallis, OR: Long-term ecological research (version 35) [Dataset]. . https://doi.org/10.6073/pasta/c96875918bb9c86d330a457bf4295cd9

Davis, K. T., Dobrowski, S. Z., Holden, Z. A., Higuera, P. E., & Abatzoglou, J. T. (2019). Microclimatic buffering in forests of the future: The role of local water balance. *Ecography*, *42*(1), 1–11. https://doi.org/10.1111/ecog.03836

Davis, R., Yang, Z., Yost, A., Belongie, C., & Cohen, W. (2017). The normal fire environment—Modeling environmental suitability for large forest wildfires using past, present, and future climate normals. *Forest Ecology and Management*, *390*, 173–186. https://doi.org/10.1016/j.foreco.2017.01.027

de Frenne, P., Lenoir, J., Luoto, M., Scheffers, B. R., Zellweger, F., Aalto, J., et al. (2021). Forest microclimates and climate change: Importance, drivers and future research agenda. *Global Change Biology*, *27*(11), 2279–2297. https://doi.org/10.1111/gcb.15569

De Ridder, K., & Gallée, H. (1998). Land surface–induced regional climate change in southern Israel. *Journal of Applied Meteorology*, *37*(11), 1470–1485. https://doi.org/10.1175/1520-0450(1998)037<1470:LSIRCC>2.0.CO;2

Dobrowski, S. Z. (2011). A climatic basis for microrefugia: The influence of terrain on climate. *Global Change Biology*, *17*(2), 1022–1035. https://doi.org/10.1111/j.1365-2486.2010.02263.x

Ferrez, J., Davison, A. C., & Rebetez, M. (2011). Extreme temperature analysis under forest cover compared to an open field. *Agricultural and Forest Meteorology*, *151*(7), 992–1001. https://doi.org/10.1016/j.agrformet.2011.03.005

Finnigan, J. J. (1979). Turbulence in waving wheat. II. Structure of momentum transfer. *Boundary-Layer Meteorology*, *16*(3), 213–236. https://doi.org/10.1007/BF03335367

Fredriksen, R. L. (1970). *Erosion and sedimentation following road construction and timber harvest on unstable soils in three small western Oregon watersheds*. Research Papers. Pacific North western Forest and Range Experiment Station, (PNW-104).

Freundorfer, A., Rehberg, I., Law, B. E., & Thomas, C. (2019). Forest wind regimes and their implications on cross-canopy coupling. *Agricultural and Forest Meteorology*, *279*, 107696. https://doi.org/10.1016/j.agrformet.2019.107696

Frey, S. J., Hadley, A. S., Johnson, S. L., Schulze, M., Jones, J. A., & Betts, M. G. (2016). Spatial models reveal the microclimatic buffering capacity of old-growth forests. *Science Advances*, *2*(4), e1501392. https://doi.org/10.1126/sciadv.1501392

Froelich, N. J., & Schmid, H. P. (2006). Flow divergence and density flows above and below a deciduous forest: Part II. Below-canopy thermo-topographic flows. *Agricultural and Forest Meteorology*, *138*(1–4), 29–43. https://doi.org/10.1016/j.agrformet.2006.03.013

Geiger, R., Aron, R. H., & Todhunter, P. (2009). *The climate near the ground*. Rowman & Littlefield.

Gronsdahl, S., Moore, R. D., Rosenfeld, J., McCleary, R., & Winkler, R. (2019). Effects of forestry on summertime low flows and physical fish habitat in snowmelt-dominant headwater catchments of the Pacific Northwest. *Hydrological Processes*, *33*(25), 3152–3168. https://doi.org/10.1002/hyp.13580

Halpern, C. B., & Franklin, J. F. (1990). Physiognomie development of Pseudotsuga forests in relation to initial structure and disturbance intensity. *Journal of Vegetation Science*, *1*(4), 475–482. https://doi.org/10.2307/3235781

Hansen, M. C., Potapov, P. V., Moore, R., Hancher, M., Turubanova, S. A., Tyukavina, A., et al. (2013). High-resolution global maps of 21st-century forest cover change. *Science*, *342*(6160), 850–853. https://doi.org/10.1126/science.1244693

Harr, R. D. (1983). Potential for augmenting water yield through forest practices in Western Washington and Western Oregon 1. *Journal of the American Water Resources Association*, *19*(3), 383–393. https://doi.org/10.1111/j.1752-1688.1983.tb04595.x

Hersbach, H., Bell, B., Berrisford, P., Hirahara, S., Horányi, A., Muñoz-Sabater, J., et al. (2020). The ERA5 global reanalysis. *Quarterly Journal of the Royal Meteorological Society*, *146*(730), 1999–2049. https://doi.org/10.1002/qj.3803

Hicks, B. J., Beschta, R. L., & Harr, R. D. (1991). Long-term changes in streamflow following logging in Western Oregon and associated fisheries implications 1. *Journal of the American Water Resources Association*, *27*(2), 217–226. https://doi.org/10.1111/j.1752-1688.1991.tb03126.x

Holden, Z. A., Swanson, A., Klene, A. E., Abatzoglou, J. T., Dobrowski, S. Z., Cushman, S. A., et al. (2016). Development of high-resolution (250 m) historical daily gridded air temperature data using reanalysis and distributed sensor networks for the US Northern Rocky Mountains. *International Journal of Climatology*, *36*(10), 3620–3632. https://doi.org/10.1002/joc.4580

Hood, E., Gooseff, M. N., & Johnson, S. L. (2006). Changes in the character of stream water dissolved organic carbon during flushing in three small watersheds, Oregon. *Journal of Geophysical Research-Biogeosciences*, *111*(G1), G01007. https://doi.org/10.1029/2005JG000082

Hosker, R. P., Jr., Nappo, C. P., Jr., & Hanna, S. R. (1974). Diurnal variation of the thermal structure in a pine plantation. *Agricultural Meteorology*, *13*(2), 259–265. https://doi.org/10.1016/0002-1571(74)90053-3

Hughes, L. (2000). Biological consequences of global warming: Is the signal already apparent? *Trends in Ecology & Evolution*, *15*(2), 56–61. https://doi.org/10.1016/S0169-5347(99)01764-4

Jensen, D. D., Nadeau, D. F., Hoch, S. W., & Pardyjak, E. R. (2016). Observations of near-surface heat-flux and temperature profiles through the early evening transition over contrasting surfaces. *Boundary-Layer Meteorology*, *159*(3), 567–587. https://doi.org/10.1007/s10546-015-0067-z

Jones, J. A., & Hammond, J. C. (2020). River management response to multi-decade changes in timing of reservoir inflows, Columbia River Basin, USA. *Hydrological Processes*, *34*(25), 4814–4830. https://doi.org/10.1002/hyp.13910

Juang, J. Y., Katul, G. G., Siqueira, M., Stoy, P. C., Palmroth, S., McCarthy, H. R., et al. (2006). Modeling night time ecosystem respiration from measured CO_2 concentration and air temperature profiles using inverse methods. *Journal of Geophysical Research*, *111*(D8), D08S05. https://doi.org/10.1029/2005JD005976

Karlsson, I. M. (2000). Nocturnal air temperature variations between forest and open areas. *Journal of Applied Meteorology*, *39*(6), 851–862. https://doi.org/10.1175/1520-0450(2000)039<0851:NATVBF>2.0.CO;2

Kiefer, M. T., & Zhong, S. (2013). The effect of sidewall forest canopies on the formation of cold-air pools: A numerical study. *Journal of Geophysical Research: Atmospheres*, *118*(12), 5965–5978. https://doi.org/10.1002/jgrd.50509

Kiefer, M. T., & Zhong, S. (2015). The role of forest cover and valley geometry in cold-air pool evolution. *Journal of Geophysical Research: Atmospheres*, *120*(17), 8693–8711. https://doi.org/10.1002/2014JD022998

Launiainen, S., Vesala, T., Mölder, M., Mammarella, I., Smolander, S., Rannik, Ü., et al. (2007). Vertical variability and effect of stability on turbulence characteristics down to the floor of a pine forest. *Tellus B: Chemical and Physical Meteorology*, *59*(5), 919–936. https://doi.org/10.1111/j.1600-0889.2007.00313.x

Lefsky, M. A., Cohen, W. B., Acker, S. A., Parker, G. G., Spies, T. A., & Harding, D. (1999). Lidar remote sensing of the canopy structure and biophysical properties of Douglas-fir Western hemlock forests. *Remote Sensing of Environment*, *70*(3), 339–361. https://doi.org/10.1016/S0034-4257(99)00052-8

Lembrechts, J. J., & Lenoir, J. (2020). Microclimatic conditions anywhere at any time. *Global Change Biology*, *26*(2), 337–339. https://doi.org/10.1111/gcb.14942

Lenoir, J., Hattab, T., & Pierre, G. (2017). Climatic microrefugia under anthropogenic climate change: Implications for species redistribution. *Ecography*, *40*(2), 253–266. https://doi.org/10.1111/ecog.02788

Leuzinger, S., & Körner, C. (2007). Tree species diversity affects canopy leaf temperatures in a mature temperate forest. *Agricultural and Forest Meteorology*, *146*(1–2), 29–37. https://doi.org/10.1016/j.agrformet.2007.05.007

Lundquist, J. D., Pepin, N., & Rochford, C. (2008). Automated algorithm for mapping regions of cold-air pooling in complex terrain. *Journal of Geophysical Research*, *113*(D22), D22107. https://doi.org/10.1029/2008JD009879

Lutz, J. A., & Halpern, C. B. (2006). Tree mortality during early forest development: A long-term study of rates, causes, and consequences. *Ecological Monographs*, *76*(2), 257–275. https://doi.org/10.1890/0012-9615(2006)076[0257:tmdefd]2.0.co;2

Menne, M. J., Williams, C. N., Jr., & Vose, R. S. (2009). The US Historical Climatology Network monthly temperature data, version 2. *Bulletin of the American Meteorological Society*, *90*(7), 993–1008. https://doi.org/10.1175/2008BAMS2613.1

Minder, J. R., Mote, P. W., & Lundquist, J. D. (2010). Surface temperature lapse rates over complex terrain: Lessons from the Cascade Mountains. *Journal of Geophysical Research*, *115*(D14), D14122. https://doi.org/10.1029/2009JD013493

Moon, K., Duff, T. J., & Tolhurst, K. G. (2019). Sub-canopy forest winds: Understanding wind profiles for fire behaviour simulation. *Fire Safety Journal*, *105*, 320–329. https://doi.org/10.1016/j.firesaf.2016.02.005

Moore, G. W., Bond, B. J., Jones, J. A., Phillips, N., & Meinzer, F. C. (2004). Structural and compositional controls on transpiration in 40-and 450-year-old riparian forests in Western Oregon, USA. *Tree Physiology*, *24*(5), 481–491. https://doi.org/10.1093/treephys/24.5.481

Muñoz-Sabater, J., Dutra, E., Agustí-Panareda, A., Albergel, C., Arduini, G., Balsamo, G., et al. (2021). ERA5-Land: A state-of-the-art global reanalysis dataset for land applications. *Earth system science data discussions*. Copernicus GmbH, 1–50. https://doi.org/10.5194/essd-2021-82

Nadeau, D. F., Oldroyd, H. J., Pardyjak, E. R., Sommer, N., Hoch, S. W., & Parlange, M. B. (2018). Field observations of the morning transition over a steep slope in a narrow alpine valley. *Environmental Fluid Mechanics*, *20*(5), 1199–1220. https://doi.org/10.1007/s10652-018-9582-z

Nadeau, D. F., Pardyjak, E. R., Higgins, C. W., Huwald, H., & Parlange, M. B. (2012). Flow during the evening transition over steep Alpine slopes. *Quarterly Journal of the Royal Meteorological Society*, *139*(672), 607–624. https://doi.org/10.1002/qj.1985

NOAA National Centers for Environmental Information, State of the Climate: Drought for Annual. (2012). published online January 2013 Retrieved from https://www.ncdc.noaa.gov/sotc/drought/201213

Oke, T. R. (2002). *Boundary layer climates* (pp. 178–179). Routledge.

Oldroyd, H. J., Pardyjak, E. R., Higgins, C. W., & Parlange, M. B. (2016). Buoyant turbulent kinetic energy production in steep-slope katabatic flow. *Boundary-Layer Meteorology*, *161*(3), 405–416. https://doi.org/10.1007/s10546-016-0184-3

Perry, T. D., & Jones, J. A. (2017). Summer streamflow deficits from regenerating Douglas-fir forest in the Pacific Northwest, USA. *Ecohydrology*, *10*(2), e1790. https://doi.org/10.1002/eco.1790

Pypker, T. G., Unsworth, M. H., Lamb, B., Allwine, E., Edburg, S., Sulzman, E., et al. (2007). Cold air drainage in a forested valley: Investigating the feasibility of monitoring ecosystem metabolism. *Agricultural and Forest Meteorology*, *145*(3–4), 149–166. https://doi.org/10.1016/j.agrformet.2007.04.016

Raynor, G. S. (1971). Wind and temperature structure in a coniferous forest and a contiguous field. *Forest Science*, *17*(3), 351–363. https://doi.org/10.1093/forestscience/17.3.351

Ritchie, M. W., Skinner, C. N., & Hamilton, T. A. (2007). Probability of tree survival after wildfire in an interior pine forest of northern California: Effects of thinning and prescribed fire. *Forest Ecology and Management*, *247*(1–3), 200–208. https://doi.org/10.1016/j.foreco.2007.04.044

Rupp, D. E., Li, S., Mote, P. W., Shell, K. M., Massey, N., Sparrow, S. N., et al. (2017). Seasonal spatial patterns of projected anthropogenic warming in complex terrain: A modeling study of the Western US. *Climate Dynamics*, *48*(7–8), 2191–2213. https://doi.org/10.1007/s00382-016-3200-x

Rupp, D. E., Shafer, S. L., Daly, C., Jones, J. A., & Frey, S. J. (2020). Temperature gradients and inversions in a forested Cascade Range basin: Synoptic-to local-scale Controls. *Journal of Geophysical Research: Atmospheres*, *125*(23), e2020JD032686. https://doi.org/10.1029/2020JD032686

Schmidli, J. (2013). Daytime heat transfer processes over mountainous terrain. *Journal of the Atmospheric Sciences*, *70*(12), 4041–4066. https://doi.org/10.1175/JAS-D-13-083.1

Segura, C., Bladon, K. D., Hatten, J. A., Jones, J. A., Hale, V. C., & Ice, G. G. (2020). Long-term effects of forest harvesting on summer low flow deficits in the Coast Range of Oregon. *Journal of Hydrology*, *585*, 124749. https://doi.org/10.1016/j.jhydrol.2020.124749

Shaw, R. H., Tavangar, J., & Ward, D. P. (1983). Structure of the Reynolds stress in a canopy layer. *Journal of Climate and Applied Meteorology*, *22*(11), 1922–1931. https://doi.org/10.1175/1520-0450(1983)022<1922:SOTRSI>2.0.CO;2

Spies, T. A., Long, J. W., Charnley, S., Hessburg, P. F., Marcot, B. G., Reeves, G. H., et al. (2019). Twenty-five years of the northwest forest plan: What have we learned? *Frontiers in Ecology and the Environment*, *17*(9), 511–520. https://doi.org/10.1002/fee.2101

Staebler, R. M., & Fitzjarrald, D. R. (2005). Measuring canopy structure and the kinematics of subcanopy flows in two forests. *Journal of Applied Meteorology*, *44*(8), 1161–1179. https://doi.org/10.1175/JAM2265.1

Stull, R. B. (2012). *An Introduction to Boundary Layer Meteorology* (Vol. 13). Springer Science & Business Media.

Thomas, C. (2017). Advanced resolution canopy FLOw (ARCFLO) experiment employing the SUbcanopy sonic anemometer network (SUSAN) in WS01 of the HJ Andrews experimental forest, July-September 2012 (version 2) [Dataset]. . https://doi.org/10.6073/pasta/e1dcac713961e62c3aaad2816bbf7780

Thomas, C., & Foken, T. (2007). Flux contribution of coherent structures and its implications for the exchange of energy and matter in a tall spruce canopy. *Boundary-Layer Meteorology*, *123*(2), 317–337. https://doi.org/10.1007/s10546-006-9144-7

Thomas, C., Martin, J. G., Goeckede, M., Siqueira, M. B., Foken, T., Law, B. E., et al. (2008). Estimating daytime sub-canopy respiration from conditional sampling methods applied to multi-scalar high frequency turbulence time series. *Agricultural and Forest Meteorology*, *148*(8–9), 1210–1229. https://doi.org/10.1016/j.agrformet.2008.03.002

Thomas, C. K. (2011). Variability of sub-canopy flow, temperature, and horizontal advection in moderately complex terrain. *Boundary-Layer Meteorology*, *139*(1), 61–81. https://doi.org/10.1007/s10546-010-9578-9

Thomas, C. K., Martin, J. G., Law, B. E., & Davis, K. (2013). Toward biologically meaningful net carbon exchange estimates for tall, dense canopies: Multi-level eddy covariance observations and canopy coupling regimes in a mature douglas-fir forest in Oregon. *Agricultural and Forest Meteorology*, *173*, 14–27. https://doi.org/10.1016/j.agrformet.2013.01.001

Thomas, C. K., & Smoot, A. R. (2013). An effective, economic, aspirated radiation shield for air temperature observations and its spatial gradients. *Journal of Atmospheric and Oceanic Technology*, *30*(3), 526–537. https://doi.org/10.1175/JTECH-D-12-00044.1

Tóta, J., Roy Fitzjarrald, D., & da Silva Dias, M. A. (2012). Amazon rainforest exchange of carbon and sub-canopy air flow: Manaus LBA site—a complex terrain condition. *The Scientific World Journal*, 1–19. https://doi.org/10.1100/2012/165067

Vickers, D., & Thomas, C. K. (2013). Some aspects of the turbulence kinetic energy and fluxes above and beneath a tall open pine forest canopy. *Agricultural and Forest Meteorology*, *181*, 143–151. https://doi.org/10.1016/j.agrformet.2013.07.014

Vickers, D., & Thomas, C. K. (2014). Observations of the scale-dependent turbulence and evaluation of the flux–gradient relationship for sensible heat for a closed Douglas-fir canopy in very weak wind conditions. *Atmospheric Chemistry and Physics*, *14*(18), 9665–9676. https://doi.org/10.5194/acp-14-9665-2014

Wang, X., Wang, C., & Li, Q. (2015). Wind regimes above and below a temperate deciduous forest canopy in complex terrain: Interactions between slope and valley winds. *Atmosphere*, *6*(1), 60–87. https://doi.org/10.3390/atmos6010060

Whiteman, C. D. (1982). Breakup of temperature inversions in deep mountain valleys: Part I. Observations. *Journal of Applied Meteorology*, *21*(3), 270–289. https://doi.org/10.1175/1520-0450(1982)021<0270:BOTIID>2.0.CO;2

Whiteman, C. D. (1990). Observations of thermally developed wind systems in mountainous terrain. In *Atmospheric processes over complex terrain* (pp. 5–42). American Meteorological Society. https://doi.org/10.1007/978-1-935704-25-6_2